NANO · MICRO small
www.small-journal.com

Lanthanide-Doped Core@Multishell Nanoarchitectures: Multimodal Excitable Upconverting/Downshifting Luminescence and High-Level Anti-Counterfeiting

*Hai Huang, Jiangkun Chen, Yutong Liu, Jidong Lin, Shaoxiong Wang, Feng Huang, and Daqin Chen**

The development of luminescent materials with concurrent multimodal emissions is a great challenge to improve security and data storage density. Lanthanide-doped nanocrystals are particularly appropriate for such applications for their abundant intermediate energy states and distinguishable spectroscopic profiles. However, traditional lanthanide luminescent nanoparticles have a limited capacity for information storage or complexity to shield against counterfeiting. Herein, it is demonstrated that the combination of upconverting and downshifting emissions in a particulate designed lanthanide-doped core@multishell nanoarchitecture allows the generation of multicolor dual-modal luminescence over a wide spectral range for complex information storage. Precise control of lanthanide dopants distribution in the core and distinct shells enables simultaneous excitation of 980/808 nm focusing/defocusing laser and 254 nm light and produces complex upconverting emissions from Er, Tm, Eu, and Tb via multiphoton energy transfer processes and downshifting emissions from Eu and Tb via efficient energy transfer from Ce to Eu/Tb in Gd-assisted lattices. It is experimentally proven that multiple visualized anti-counterfeit and information encryption with facile decryption and authentication using screen-printing inks containing the present core@multishell nanocrystals are practically applicable by selecting different excitation modes.

1. Introduction

Counterfeiting is currently becoming a serious threat to every aspect of the global markets. Thus, advanced security strategies and anti-counterfeiting techniques are highly desirable to ensure the authentic items difficult to be replicated. It has been recently reported that the counterfeiting market was about $107 billion in 2016, will grow at a rate of 14.0% and can finally reach $206 billion by 2021.[1] Conventional product packaging techniques, including watermarking/stamping, digital signature standard, barcoding and box seal, have been gradually replaced for their easy duplication.[2,3] Fluorescence printing patterns can promise a high-level security and safeguarding valuable documents due to its tunable and designable emissive properties.[4–6] Traditional luminescent materials, such as dye molecules and quantum dots, can produce multicolor emissions, but the shortages of easy photobleaching and obvious polluting limit their practical application in the anti-counterfeiting field.[7–10]

As an alternative, lanthanide (Ln^{3+}) doped luminescent materials excitable by ultraviolet (UV) light or near-infrared (NIR) laser have been demonstrated to be suitable for concealing factual data and shielding against counterfeiting by taking advantage of their unique optical characteristics of color-tunable emissions, sharp emission bands, long luminescent lifetimes (micro- to milli-seconds) and low toxicity.[11–14] Currently, two kinds of Ln-based light conversions, i.e., downshifting (DS) and upconversion (UC), have been adopted in commercial anti-counterfeiting.[15–22] DS is a photoluminescence (PL) process where one high-energy photon is converted into a low-energy photon, while UC is an anti-Stokes process where low-energy radiation is converted into high-energy emitting light via a successive two- or multi-photon absorption mechanism.[23–25] For instance, Eu-doped DS phosphors have been employed in Euro banknotes to produce visible PL after placing a banknote under the excitation of UV lamp. Yb/Er-doped UC phosphors have been adopted in Chinese RMB banknotes to produce yellow UC luminescence after putting a banknote under the irradiation of

H. Huang, J. K. Chen, Y. T. Liu, J. D. Lin, S. X. Wang, Prof. F. Huang, Prof. D. Q. Chen
College of Physics and Energy
Fujian Normal University
Fujian Provincial Key Laboratory of Quantum Manipulation and New Energy Materials
Fuzhou 350117, China
E-mail: dqchen@fjnu.edu.cn

H. Huang, J. K. Chen, Y. T. Liu, J. D. Lin, S. X. Wang, Prof. F. Huang, Prof. D. Q. Chen
Fujian Provincial Collaborative Innovation Center for Advanced High-Field Superconducting Materials and Engineering
Fuzhou 350117, China

Prof. F. Huang, Prof. D. Q. Chen
Fujian Provincial Engineering Technology Research Center of Solar Energy Conversion and Energy Storage
Fuzhou 350117, China

The ORCID identification number(s) for the author(s) of this article can be found under https://doi.org/10.1002/smll.202000708.

DOI: 10.1002/smll.202000708

980 nm laser.[26,27] Notably, UC materials with excellent photostability and low background autofluorescence have been developed as a new category of luminescent inks that have become promising alternatives to organic dyes and quantum dots applied in anti-counterfeiting.[14]

Despite of these progresses, it remains a formidable challenge to produce finely tunable DS and UC emissions simultaneously in one material for anti-counterfeiting application, which is believed to be beneficial to improve security and data storage capacity. Generally, Yb-Tm, Yb-Er, and Yb-Er-Tm dopant combinations are used to produce blue/green/red (BGR) tricolor UC emissions;[24] Ce–Tb and Ce–Eu dopant combinations are employed to yield green and red DS emissions.[28,29] Yb and Ce in these couples are sensitizers to improve UC and DS emissions for their large absorption cross-sections. Unfortunately, it is formidably hard to concurrently achieve intense DS emissions of Tb/Eu and UC emission of Er/Tm via simply codoping them in one host owing to the occurrence of luminescent coquenching. One effective route to address this issue is to construct core@shell nanoarchitecture where Ln^{3+} activators can be spatially separated via doping in core and shell to avoid adverse energy transfer (ET) or cross relaxation among them.[30–36] Recently, Kaczmarek and Deun prepared various combinations of Ln-doped core@shell nanocrystals (NCs), i.e., $LiLuF_4$: Yb/Ln (Ln = Er, Ho, Tm)@$LiYF_4$: Ce/Ln (Ln = Eu, Tb), to produce efficient UC and DS emissions under the excitation of 980 nm NIR laser and/or UV lamp for promising application in multimode anticounterfeiting.[37] However, the UC emissions came from routine Er, Ho, or Tm 4f–4f transitions, which will be easily discerned and imitated, and no proof-of-concept experiment concerning anticounterfeit application was carried out.

In this work, we design a novel lanthanide-doped core@multishell nanoarchitecture to create multimode high-security anticounterfeiting NCs (**Figure 1**). Compared to the previously reported one, upconverting emissions from Er, Tm and Eu/Tb can be simultaneously achieved by combining $NaYF_4$: Nd/Yb@$NaYF_4$: Yb/Er@$NaGdF_4$: Yb/Tm core@shell@shell structures with $NaGdF_4$: A@$NaYF_4$ (A = Eu, Tb, Eu/Tb, Ce/Eu, Ce/Tb, Ce/Eu/Tb) shell@shell layers. $NaYF_4$ is chosen as UC host for their efficient UC emissions after doping Yb/Er couple.[24] $NaGdF_4$ layer is adopted in the second and third shells to enable energy migration UC from Tm to Eu/Tb with the assistance of Gd ions. As schematically illustrated in Figure 1a,b, Nd, Yb and Ce sensitizers are doped to enable to excite the products via three diverse wavelengths (single 254, 980, or 808 nm) or the combined UV/NIR wavelengths (254/980 nm or 254/808 nm) to synchronously produce both DS and UC emissions. Herein, Er and Tm activators are doped to yield red, green and blue (RGB) tricolor UC emissions via the classic energy transfer UC processes (Figure 1a,b; Figures S1 and S2, Supporting Information); Eu and Tb activators are doped to yield red and green DS emissions (Figure 1a,b). Notably, taking advantage of efficient energy migration from Tm to Gd and finally to Eu/Tb, Eu and Tb emitting centers can also produce UC emissions (Figure 1a,b). The simultaneously excited Er, Tm, and Eu/Tb ions in the core@shell structures can lead to adjustable UC colors under 980 or 808 nm excitation and show interesting laser-focusing/defocusing sensitive UC luminescence (Figure 1b,c). Combined with UV-excitable DS emissions, the present core@shell NCs with suppressed coquenching DS/UC effect, could allow the development of novel and advanced multimode security technologies. Finally, the demonstration experiments for the present CSSSS NCs in multimodal anticounterfeit and information encryption/decryption are performed. As far as we know, this is the first report concerning Er/Tm/Eu/Tb UC and Eu/Tb DS core@multishell NCs for security applications.

2. Results and Discussion

All the core@shell samples were synthesized via a layer-by-layer coprecipitation method and the detailed procedures can be found in experimental section. X-ray diffraction (XRD) patterns of core and core@shell samples with 1–4 shells (denoted as C, CS, CSSS, CSSS and CSSSS, respectively) are presented in Figure S3 in the Supporting Information. All the products are well indexed to pure hexagonal β-$NaYF_4$ (JCPDS No. 16-0334) phase, and the corresponding diffraction peaks are gradually sharpened after growing four layers, which suggests an increase in the particle size from core to core@multishell samples. Scanning electron microscopy (SEM) micrographs (Figure S4, Supporting Information) evidence that the core NCs are monodispersed with the mean sizes of ≈20 nm and the particles sizes increase to 26, 37, 44, and ≈55 nm (diameter) × ≈45 nm (length, along c axis) for CS, CSS, CSSS and CSSSS NCs, respectively. Transmission electron microscopy (TEM, Figure S5, Supporting Information) and high-angle annular dark-field (HAADF) scanning TEM (STEM, **Figure 2**a) images demonstrate obvious contrast for the core and the outer shells in the CSSSS nanoarchitecture. Owing to the large difference of atomic number between Y (Z = 39) and Gd (Z = 64), the obvious contrast for the Gd-contained shell (bright) and the Y-contained core or shell (dark) is clearly discernable (Figure 2a), verifying the successful growth of multishell on the surface core. High-resolution TEM (HRTEM) images for a typical CSSSS NC (Figure 2b,c) and the corresponding selected area electron diffraction (SAED) patterns confirm its single-crystalline nature with high-crystallinity. The lattice fringes are well resolved, and the d-spacings about 0.52 and 0.30 nm are observed, which can be assigned to the (100) and (110) planes of hexagonal $NaYF_4$. All these results confirm that the as-prepared CSSSS NCs are nanoplates, which show a preferred growth along [0001] and are enclosed by {10-10} and {0001} facets. Evidently, energy dispersive X-ray (EDX) elemental mappings of Na, F, Y, Gd, Nd, Yb, Ce, and Tb performed on four typical CSSSS particles (Figure 2d–l) reveal that Nd ions are confined inside the core, Gd/Ce/Tb ions locate in the shell, and Na/F ions uniformly in the core and shell layers. These results verify successful formation of the designed $NaYF_4$: Nd/Yb@$NaYF_4$: Yb/Er@$NaGdF_4$: Yb/Tm@$NaGdF_4$: Ce/Tb@$NaYF_4$ CSSSS nanoarchitecture.

Taking $NaYF_4$: Nd/Yb@$NaYF_4$: Yb/Er@$NaGdF_4$: Yb/Tm@$NaGdF_4$: Eu@$NaYF_4$ core@shell product as a typical example, we investigated UC emissive properties after layer-by-layer growth of different shells. For Nd/Yb: $NaYF_4$ core, 980 nm emission assigned to Yb^{3+} $^2F_{5/2} \rightarrow {}^2F_{7/2}$ transition is obviously observed upon 808 nm laser excitation (corresponding to

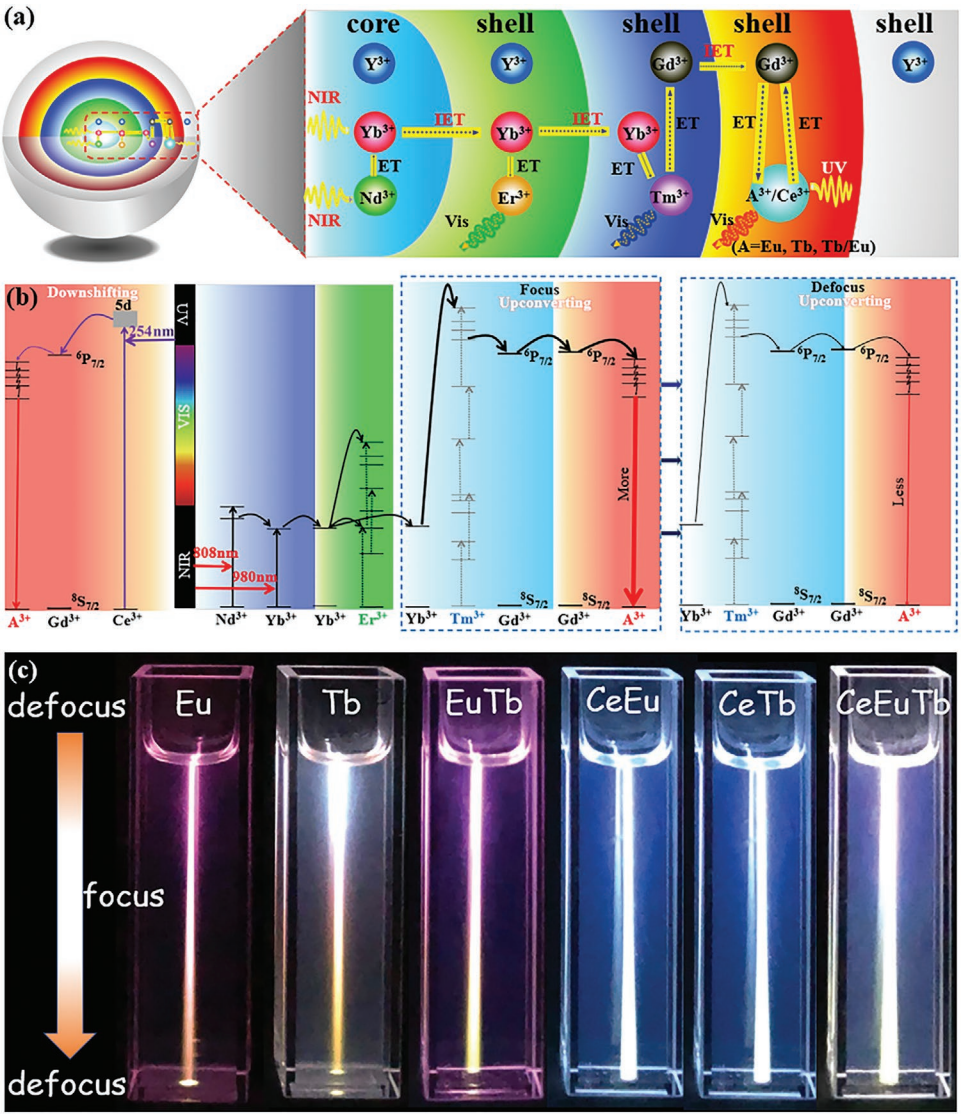

Figure 1. a) Schematic core@multishell nanoarchitectures of $NaYF_4$: Nd/Yb@$NaYF_4$: Yb/Er@$NaGdF_4$: Yb/Tm@$NaGdF_4$: A@$NaYF_4$ (A = Eu, Tb, Eu/Tb, Ce/Eu, Ce/Tb, Ce/Tb/Eu). In these core@shell structures, Nd/Yb are codoped in $NaYF_4$ core to enable the excitation of 808 nm/980 nm laser, Yb/Er and Yb/Tm are doped in different shells (the first $NaYF_4$ shell and the second $NaGdF_4$ shell, respectively) to spatially separate them to induce intense Er and Tm UC emissions, Ce/Tb/Eu are doped in the third $NaGdF_4$ shell to produce dual-modal DS/UC emissions, and the fourth $NaYF_4$ inert shell is used to reduce surface quenching effect. Notably, $NaGdF_4$ host is adopted in the second and third shells to enable energy migration UC from Tm to Eu/Tb with the assistance of Gd ions. ET represents energy transfer in the individual core or shell, IET represents interface energy transfer from one shell to the next one. b) Simplified energy level diagrams of Nd, Yb, Er, Tm, Ce, Gd, and A (A = Eu, Tb) as well as the proposed mechanisms for the simultaneous achievement of UC/DS emission under the excitation of 980 nm/808 nm laser and 254 UV light. c) UC emissive photographs for the represented core@shell NCs (from left to right: Ln dopants in the third shell are Eu, Tb, Eu/Tb, Ce/Eu, Ce/Tb, and Ce/Eu/Tb) dispersed in cyclohexane solution under the irradiation of 980 nm. The incident laser is focused in the center of the solution and the UC color changes can be easily discerned from top solution (exposure to defocusing laser) to center solution (exposure to focusing laser) and finally to bottom solution (exposure to defocusing laser).

Nd^{3+} $^4I_{9/2} \rightarrow {}^4F_{5/2}$ absorption transition), evidencing the occurrence of energy transfer from Nd to Yb in the core (**Figure 3**a). UC emission spectrum of $NaYF_4$: Nd/Yb@$NaYF_4$: Yb/Er CS sample under 808 nm laser excitation shows typical Er^{3+}: $^2H_{11/2} \rightarrow {}^4I_{15/2}$ (521 nm), $^4S_{3/2} \rightarrow {}^4I_{15/2}$ (541 nm) and $^4F_{9/2} \rightarrow {}^4I_{15/2}$ (654 nm) emissions (Figure 3b). After the growth of second $NaGdF_4$: Yb/Tm shell (CSS), extra UC bands attributed to Tm^{3+}: $^1D_2 \rightarrow {}^3F_4$ (450 nm), $^1G_4 \rightarrow {}^3H_6$ (475 nm), and $^3F_{2,3} \rightarrow {}^3H_6$ (696 nm) transitions are detected (Figure 3b). Further coating third Eu^{3+}: $NaGdF_4$ shell (CSSS) can produce characteristic Eu^{3+}: $^5D_0 \rightarrow {}^7F_1$ (590 nm) and $^5D_0 \rightarrow {}^7F_2$ (615 nm) red UC emissions (Figure 3b).

The detailed energy transfer processes responsible for simultaneous UC emissions of multiple activators (Er, Tm, Eu) upon 808 nm laser excitation in the CSSSS nanoarchitecture are proposed and schematically illustrated in Figure 1a,b and Figure S1 in the Supporting Information. The incident 808 nm lasers populate Nd^{3+} $^4F_{5/2}$ excited state via ground state absorption (GSA), followed by nonradiative relaxation to $^4F_{3/2}$ one. The energy could transfer to nearby Yb^{3+} and populate its $^2F_{5/2}$

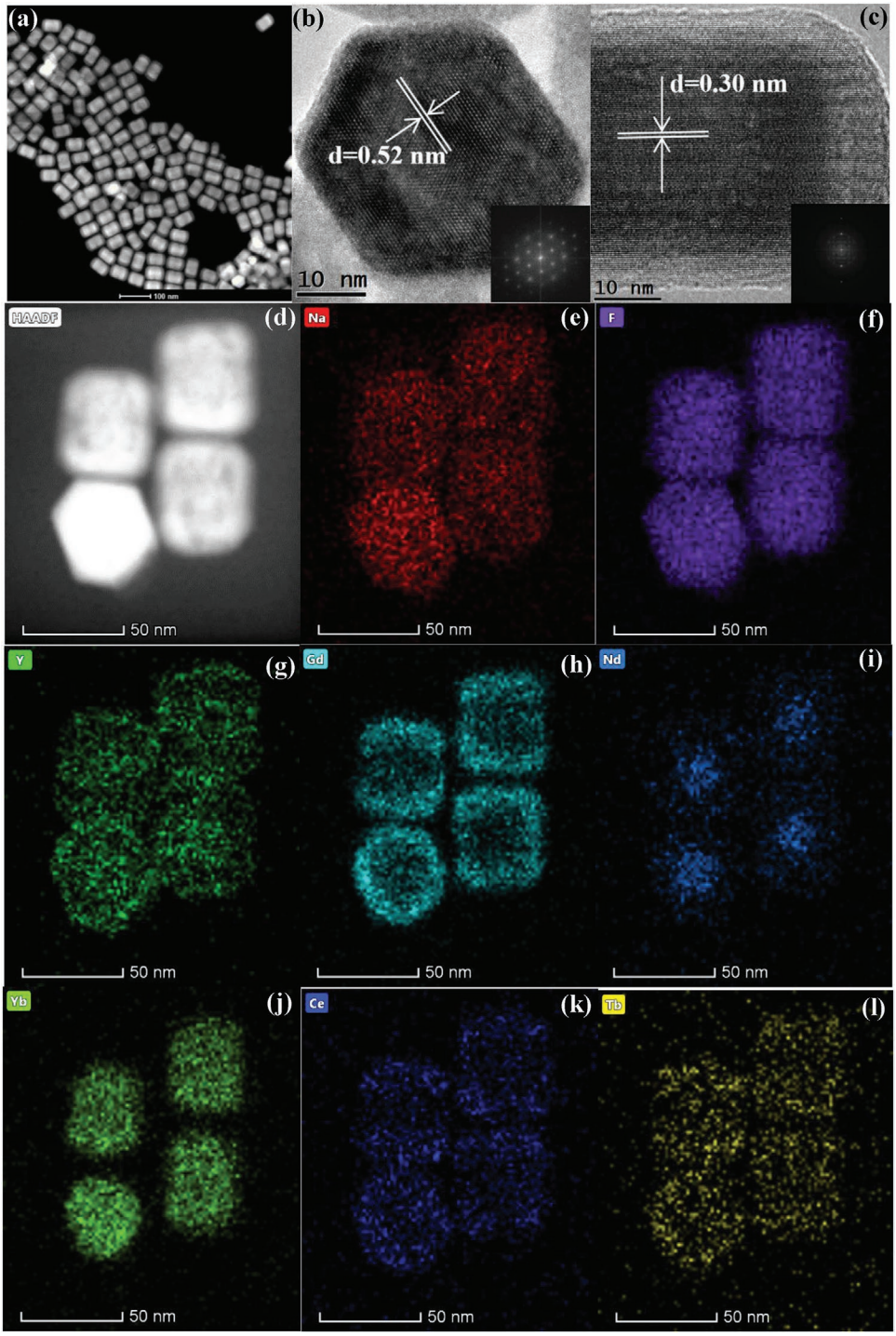

Figure 2. a) HADDF-STEM image of a typical $NaYF_4$: Nd/Yb@$NaYF_4$: Yb/Er@$NaGdF_4$: Yb/Tm@$NaGdF_4$: Ce/Tb@$NaYF_4$ CSSSS sample. HRTEM micrographs of b) top view and c) side view of an individual CSSSS NC. Insets are the corresponding fast Fourier transform (FFT) patterns. d) STEM image and EDX mappings of e) Na, f) F, g) Y, h) Gd, i) Nd, j) Yb, k) Ce, and l) Tb elements.

state through Nd^{3+}: $^4F_{3/2}$ + Yb^{3+}: $^2F_{7/2}$ → Nd^{3+}: $^4I_{11/2}$ + Yb^{3+}: $^2F_{5/2}$[38,39] and further migrate to nearby Yb^{3+} ions crossing the first $NaYF_4$: Yb/Er shell. This ET route would initiate a typical Er^{3+} UC process in the shell, where Er^{3+} ions are excited to green-emitting $^2H_{11/2}$,$^4S_{3/2}$ states and red-emitting $^4F_{9/2}$ state by ET upconversion (ETU) from Yb to Er. A remarkable decrease in Yb^{3+} decay lifetime after the growth of $NaYF_4$: Yb/Er shell on $NaYF_4$: Nd/Yb core evidences ET process from Yb to Er in the CS sample (Figure 3c). Furthermore, energy migration from Yb in first $NaYF_4$: Yb/Er shell to second $NaGdF_4$: Yb/Tm shell and subsequent ETU from Yb to Tm can populate Tm^{3+} blue-emitting $^1D_2$, $^1G_4$ states and NIR-emitting $^3F_{2,3}$ states. With the

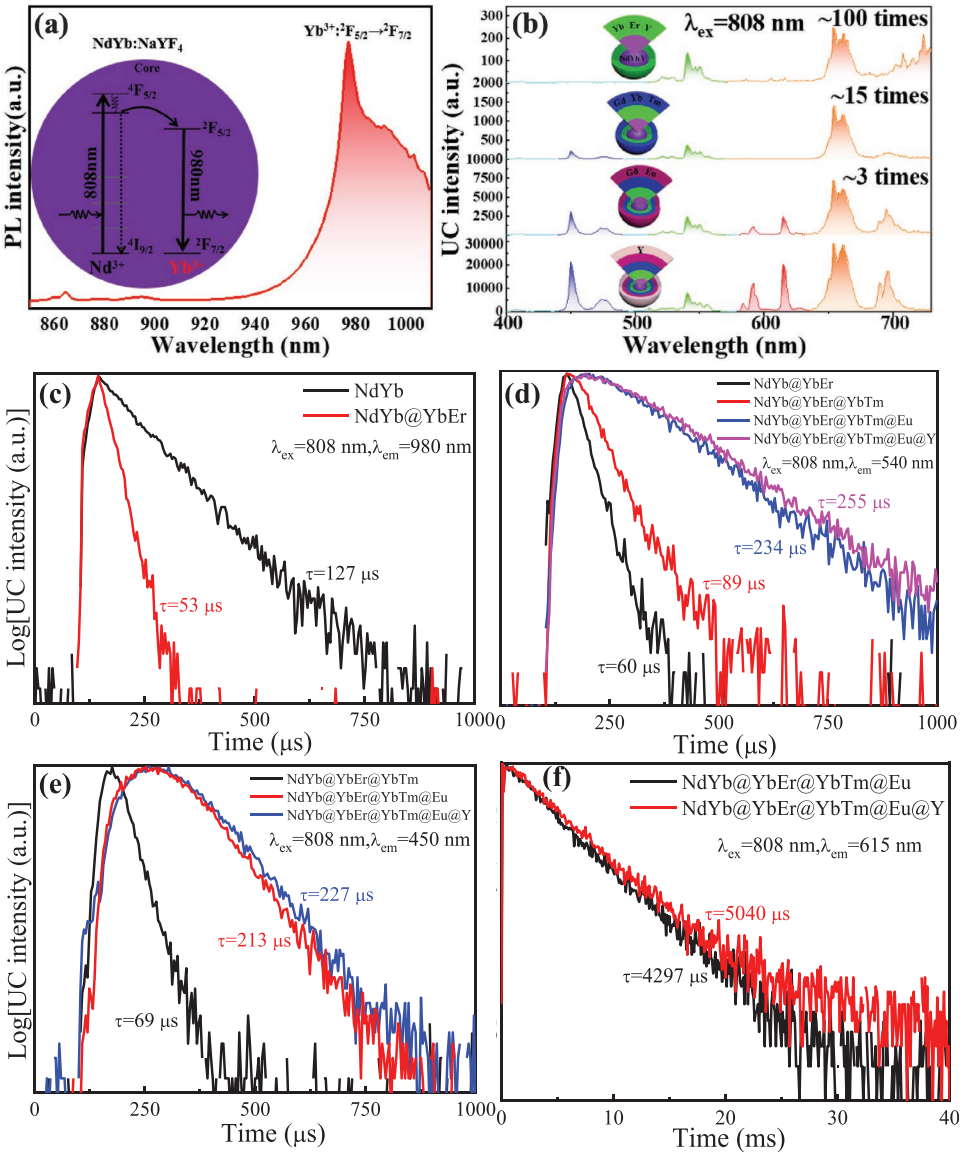

Figure 3. a) PL spectrum of $NaYF_4$: Nd/Yb core NCs under the excitation of 808 nm laser. b) UC emission spectra of core@shell samples under 808 nm laser irradiation (from top to bottom: CS, CSS, CSSS, and CSSSS). Inset is the proposed Nd → Yb energy transfer process. c) PL decay curves by monitoring Yb^{3+} $^2F_{5/2} \rightarrow {}^2F_{7/2}$ transition (980 nm emission). UC decay curves by monitoring d) Er^{3+} $^4S_{3/2} \rightarrow {}^4H_{15/2}$ transition (540 nm emission), e) Tm^{3+} $^1D_2 \rightarrow {}^3F_4$ transition (450 nm emission), and f) Eu^{3+} $^5D_0 \rightarrow {}^7F_2$ transition (615 nm emission) for the CS, CSS, CSSS, and CSSSS samples. All the decay curves are excited under 808 nm pulse laser.

growth of third $NaGdF_4$: Eu shell, energy migration process of Tm → Gd → Eu finally induces Eu^{3+} UC $^5D_0 \rightarrow {}^7F_{1,2}$ emissions. Notably, it is observed that significant enhancement in overall UC emission intensities of Er^{3+}, Tm^{3+} and Eu^{3+} activators is achieved after the growth of the corresponding shells, which is attributed to the surface passivation role of shell.[40] Specifically, Er^{3+} UC luminescence in CSSSS is about 100 times higher than that in CS; Tm^{3+} UC luminescence in CSSS is about 75 times higher than that in CSS; Eu^{3+} UC luminescence in CSSSS is about 10 times higher than that in CSSS (Figure 3b). For UC materials, a long decay lifetime usually indicates more efficient UC emissions. [41,42] As revealed in Figure 3d–f, the tendency of lifetime variation is consistent with that of UC emissive variation: UC decay lifetimes for the Er^{3+}: $^4S_{3/2}$, Tm^{3+}: $^1D_2$, and Eu^{3+} $^5D_0$ emitting states are gradually lengthened with growth of shells since the shell can protect the luminescent Ln^{3+} ions (especially those near or on the surface of NCs) from nonradiative deexcitation caused by surface defects. Similarly, UC emissions from multiple activators of Er^{3+}, Tm^{3+}, and Eu^{3+} can also be detected under the excitation of 980 nm laser, and the growth of multishell can result in a great increase in their corresponding UC emission intensities and lengthen UC decay lifetimes of Er^{3+}: $^4S_{3/2}$, Tm^{3+}: $^1D_2$, and Eu^{3+} $^5D_0$ emitting states (Figure S6, Supporting Information).

UC emission spectra for the $NaYF_4$: Nd/Yb@$NaYF_4$: Yb/Er@$NaGdF_4$: Yb/Tm@$NaGdF_4$: A@$NaYF_4$ CSSSS (A = Eu, Tb, Eu, Ce/Eu, Ce/Tb, Ce/Tb/Eu) samples upon the excitation of 980 nm laser are recorded and provided in **Figure 4**a. For

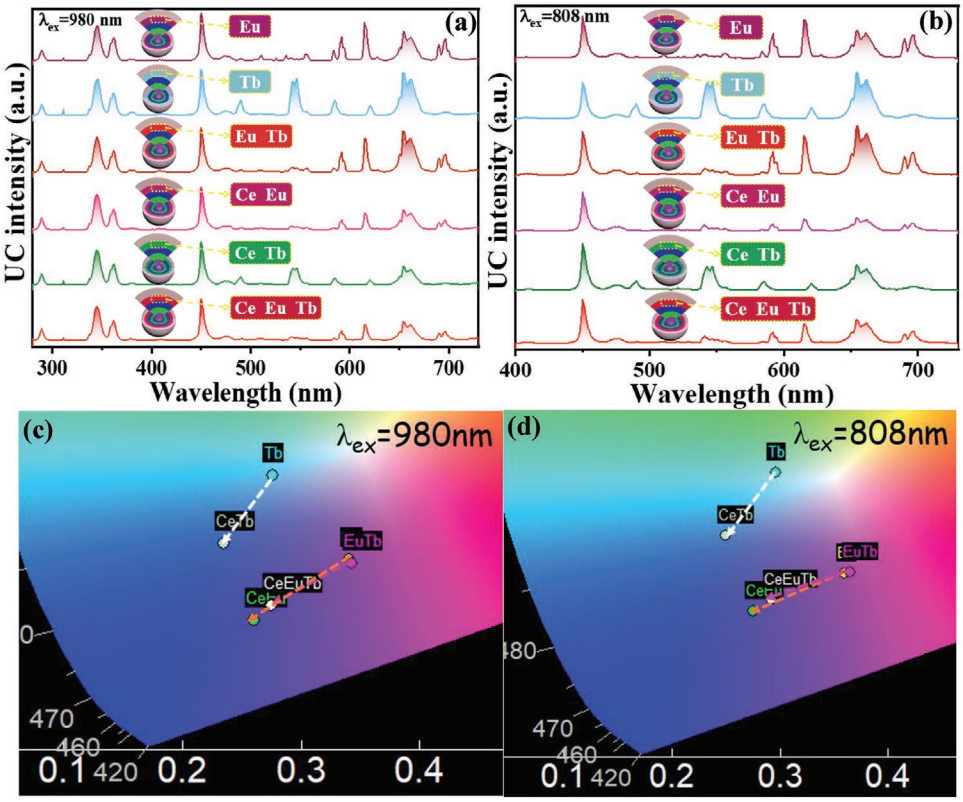

Figure 4. UC emission spectra of $NaYF_4$: Nd/Yb@$NaYF_4$: Yb/Er@$NaGdF_4$: Yb/Tm@$NaGdF_4$: A@$NaYF_4$ CSSSS (A = Eu, Tb, Eu, Ce/Eu, Ce/Tb, Ce/Tb/Eu) samples under the irradiation of a) 980 nm laser and b) 808 nm laser. c,d) UC emissive color coordinates in CIE 1931 diagrams for the corresponding CSSSS sample under 980/808 nm laser excitation.

Eu^{3+} doped in the third $NaGdF_4$ shell, multiple UC emissive bands assigned to Er^{3+}: $^4G_{11/2} \rightarrow {}^4I_{15/2}$ (383 nm), $^2H_{9/2} \rightarrow {}^4I_{15/2}$ (408 nm), $^2H_{11/2} \rightarrow {}^4I_{15/2}$ (521 nm), $^4S_{3/2} \rightarrow {}^4I_{15/2}$ (541 nm), and $^4F_{9/2} \rightarrow {}^4I_{15/2}$ (654 nm) transitions, Tm^{3+}: $^1I_6 \rightarrow {}^3H_6$ (289 nm), $^1I_6 \rightarrow {}^3F_4$ (345 nm), $^1D_2 \rightarrow {}^3H_6$ (361 nm), $^1D_2 \rightarrow {}^3F_4$ (450 nm), $^1G_4 \rightarrow {}^3H_6$ (475 nm), and $^3F_{2,3} \rightarrow {}^3H_6$ (695 nm) transitions, Gd^{3+}: $^6P_{7/2} \rightarrow {}^8S_{7/2}$ (311 nm) transition, Eu^{3+}: $^5D_2 \rightarrow {}^7F_3$ (510 nm), $^5D_1 \rightarrow {}^7F_2$ (556 nm), $^5D_0 \rightarrow {}^7F_1$ (591 nm), $^5D_0 \rightarrow {}^7F_2$ (615 nm), and $^5D_0 \rightarrow {}^7F_1$ (690 nm) transitions,[23,24] are detected in the CSSSS sample. For Tb^{3+} doped in the third $NaGdF_4$ shell, Tb^{3+}: $^5D_4 \rightarrow {}^7F_6$ (490 nm), $^5D_4 \rightarrow {}^7F_5$ (546 nm), $^5D_4 \rightarrow {}^7F_4$ (585 nm), and $^5D_4 \rightarrow {}^7F_3$ (620 nm) transitions are clearly observed besides Er^{3+} and Tm^{3+} 4f–4f transitions. All these mentioned 4f–4f transitions are tabulated in Table S1 in the Supporting Information. For Tb/Eu codoped in the third $NaGdF_4$ shell, Eu^{3+} UC emissions are dominant in the spectrum, indicating efficient UC ET from Tb^{3+} to Eu^{3+} upon 980 nm laser excitation (Figure S7, Supporting Information). As illustrated in CIE 1931 diagram (Figure 4c), Tb doped CSSSS produces UC emitting color in the cyan region, while Eu doped and Tb/Eu codoped CSSSS samples produce UC emitting color in the pink region. Indeed, Eu and Tb/Eu doped samples have similar color coordinates (Table S2, Supporting Information) and almost locate in the same region of CIE diagram (Figure 4c), confirming the occurrence of efficient Tb → Eu ET UC (Figure S7, Supporting Information). The UC quantum yield (UCQY) values for the CSSSS samples doped with Eu, Tb and Tb/Eu in the third shells obtained by integrating the characteristic emissions of Er, Tm, Eu, and Tb dopants are determined to be 2.3%, 1.9%, and 2.1% upon 980 nm laser irradiation (2.0 W cm^{-2}), respectively. Interestingly, introducing Ce^{3+} ions into the third $NaGdF_4$ shell (Ce/Eu, Ce/Tb, or Ce/Tb/Eu doped $NaGdF_4$), the corresponding emissive intensities of Eu^{3+} and Tb^{3+} activators relative to those of Tm^{3+} ones are remarkably reduced, leading to the shifting of color coordinates into blue regions (Figure 4c). Considering the conditions of energy matching between Tm^{3+} in second shell and Ce^{3+} in third shell, herein it is proposed that energy cross relaxations between Ce^{3+} and Tm^{3+} (Ce: $^2F_{5/2}$+Tm: $^3H_5$ → Ce: $^2F_{7/2}$+Tm: $^3F_4$; Ce: $^2F_{5/2}$+Tm: $^3F_{2,3}$ → Ce: $^2F_{7/2}$+Tm: $^3H_4$) occurring in the corresponding interface will reduce the ET probability from Tm^{3+} to Eu^{3+}/Tb^{3+} (Figures S8–S10, Supporting Information). Similarly, upon 808 nm excitation, multiband UC emissions from Er, Tm, Eu, Tb can be detected and introducing Ce^{3+} into third shell also results in the lowering of Eu/Tb UC luminescence and shifting of color coordinates into blue region (Figure 4b,d).

In a further experiment, we recorded laser-powder-dependent UC emission spectra. As shown in Figures S11–S14 in the Supporting Information, slight changes in UC emissive colors are found with increase of 980 or 808 nm focused laser power. This is attributed to the different multiphoton absorption UC mechanisms for Tm^{3+}, Eu^{3+}, Tb^{3+}, and Er^{3+}. Only two-photon absorption is required for Er^{3+} (green/red) UC luminescence while at least three-photon absorption is

necessary for Tm^{3+} (blue) and Eu^{3+}/Tb^{3+} (red/green) UC luminescence.[22–24,30,43] Therefore, UC emissive colors for all the CSSSS samples tend to shift towards blue region with increase of laser power, however, the color change is not significant probably owing to the easily saturated multiphoton UC absorption in the present CSSSS samples with high Yb^{3+} doping content (up to ≈60 mol%). As a comparison, benefited from the multishell structure, remarkable change of UC emissive

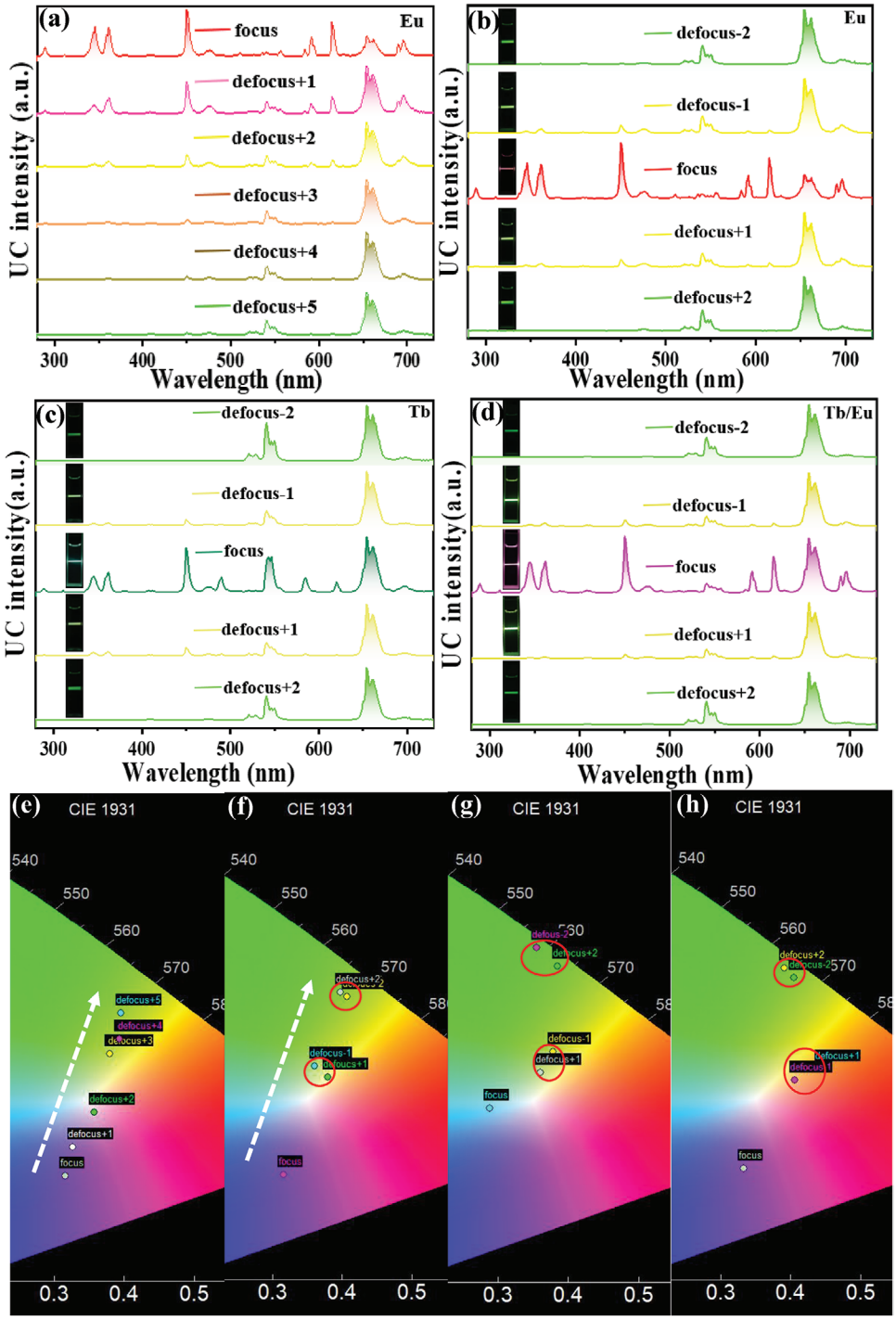

Figure 5. a) UC emission spectra for the Eu-doped CSSSS sample with increase of laser defocusing levels. The laser power density gradually increases from focus to defoucs+5 (1, 2, 3, 4, 5, and 6 W cm^{-2}). UC emission spectra for the b) Eu-doped, c) Tb-doped, and d) Tb/Eu-doped CSSSS samples upon 980 nm laser excitation in both under-focusing (defocus-1, defocus-2) and overfocusing (defocus+1, defocus+2) modes. The laser power densities are 1, 2, and 3 W cm^{-2} for the focus, defoucs±1 and defoucs±2 modes, respectively. Insets are the corresponding UC luminescent photographs for the samples dispersed in hexane solutions. e–h) UC emissive color coordinates in CIE diagrams of (a), (b), (c), and (d).

color can be achieved by simply modifying the levels of laser focusing (Figure S15, Supporting Information). Taking CSSSS doped with Eu^{3+} in third shell as a typical sample, Tm^{3+} blue and Eu^{3+} red emissions are dominant in the UC spectra when the laser is well focused on the sample, and these emissions gradually disappear while Er^{3+} green/red UC emissions become prominent with increase of laser defocusing degree (from 1 to 5, **Figure 5**a), leading to tunable UC color from blue, pink, white, yellow to green (Figure 5e; Table S3, Supporting Information). As demonstrated in Figure 5b,f and Table S4 (Supporting Information), laser irradiation in both underfocusing and overfocusing modes (Figure S15, Supporting Information) has the similar effect on UC emissive color. As expected, Tb^{3+} doped and Tb^{3+}/Eu^{3+} codoped CSSSS samples also exhibit such laser-focusing sensitive UC emissions and colors (Figure 5c,d,g,h; Tables S5 and S6, Supporting Information). These results are reasonable since the defocused incident laser has not enough energy to pump Tm to higher excited states to produce blue emissions and thus Eu/Tb red/green emission. Consequently, the Er^{3+} UC emissions become dominant with increase of defocusing level and the yielded UC emissive color gradually changes into the yellow-green region. This color variation over a wide spectral range is a unique advantage for the present core@multishell NCs to find practical application in anti-counterfeiting.

Photoluminescent (PL or DS) spectra for the CSSSS samples doped with Ce/Eu, Ce/Tb, and Ce/Tb/Eu and the related PL excitation (PLE) spectra were recorded and presented in **Figure 6**a–c. Under the excitation of 254 nm light, typical Eu^{3+} $^5D_0 \rightarrow {}^7F_J$ (J = 1, 2, 3, 4) emissions (Figure 6a) and Tb^{3+} $^5D_4 \rightarrow {}^7F_J$ (J = 6, 5, 4, 3) emissions (Figure 6b) are detected for the Ce/Eu doped and Ce/Tb doped CSSSS samples. In addition, both samples show an extra emission at 311 nm assigned to Gd^{3+} $^6P_{7/2} \rightarrow {}^8S_{7/2}$ transition. PLE spectra by monitoring Eu^{3+} 615 nm emission ($^5D_0 \rightarrow {}^7F_2$) and Tb^{3+} 545 nm emission ($^5D_4 \rightarrow {}^7F_5$) consist of one broad excitation band due to Ce^{3+} 4f → 5d absorption transition and one sharp excitation peak assigned to Gd^{3+} $^8S_{7/2} \rightarrow {}^6I_{7/2}$ absorption transition. All these results confirm efficient energy transfer from Ce^{3+} sensitizers to Gd^{3+} bridging centers and finally to Eu^{3+} or Tb^{3+} activators (Figures S8 and S9, Supporting Information), from which red or green DS luminescence yields. Notably, without the addition of Ce^{3+} sensitizers, Eu^{3+} and Tb^{3+} emissions are hardly detected in the CSSSS samples for their parity-forbidden 4f–4f absorption transitions and low absorption cross-sections.[44,45] Similar to the case of UC luminescence, Eu^{3+} DS emissions are dominant for the Ce/Tb/Eu doped sample (Figure 6c), further confirming that energy transfer from Tb^{3+} to Eu^{3+} is highly efficient in the present sample (Figure S10, Supporting Information). Distinct DS emitting colors (red, green and pink) are

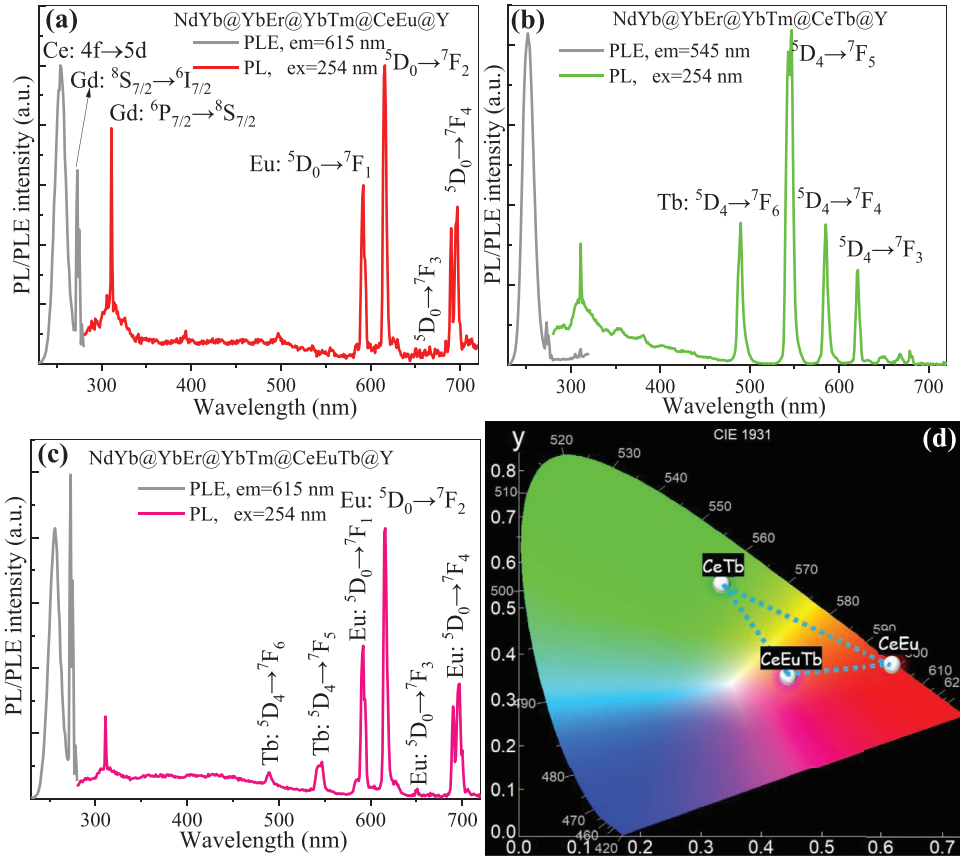

Figure 6. DS emission and excitation spectra of $NaYF_4$: Nd/Yb@$NaYF_4$: Yb/Er@$NaGdF_4$: Yb/Tm@$NaGdF_4$: Ce/A@$NaYF_4$ CSSSS samples under the excitation of 254 nm light: a) A = Eu, b) A = Tb, c) A = Tb/Eu. d) CIE diagram showing color coordinates of DS luminescence for the corresponding samples.

clearly discerned by plotting the corresponding emissive color coordinates in CIE diagram (Figure 6d; Table S7, Supporting Information).

Interestingly, it is feasible to tune DS/UC combined luminescence of CSSSS over a broad range upon simultaneous excitation of 980 nm laser and UV light (Figure S15, Supporting Information). Herein, 980 nm laser power is fixed and the power of incident UV excitation light (254 nm) is gradually increased. As shown in **Figure 7**a–c, the luminescent spectra consist of Er/Tm/A (A = Eu, Tb) UC emission bands and Gd/A (A = Eu, Tb) DS emission bands for the CSSSS samples doped with Ce/Eu, Ce/Tb, or Ce/Tb/Eu in the third shell. With increase of UV light power, Gd/Eu or Gd/Tb DS emissions monotonously enhance via energy transfer from Ce to Gd and then to Eu or Tb, while Er/Tm UC emissions remain unchanged, leading to the shift of emissive color from blue to white and finally to red for the Ce/Eu doped CSSSS sample (Figure 7d; Table S8, Supporting Information), from blue to cyan and finally to green for the Ce/Tb doped CSSSS sample (Figure 7e; Table S9, Supporting Information), and from blue to pink for the Ce/Tb/Eu doped CSSSS sample (Figure 7f; Table S10, Supporting Information).

Finally, we demonstrate the practical application for the present CSSSS NCs in anti-counterfeiting. As a proof-of-concept

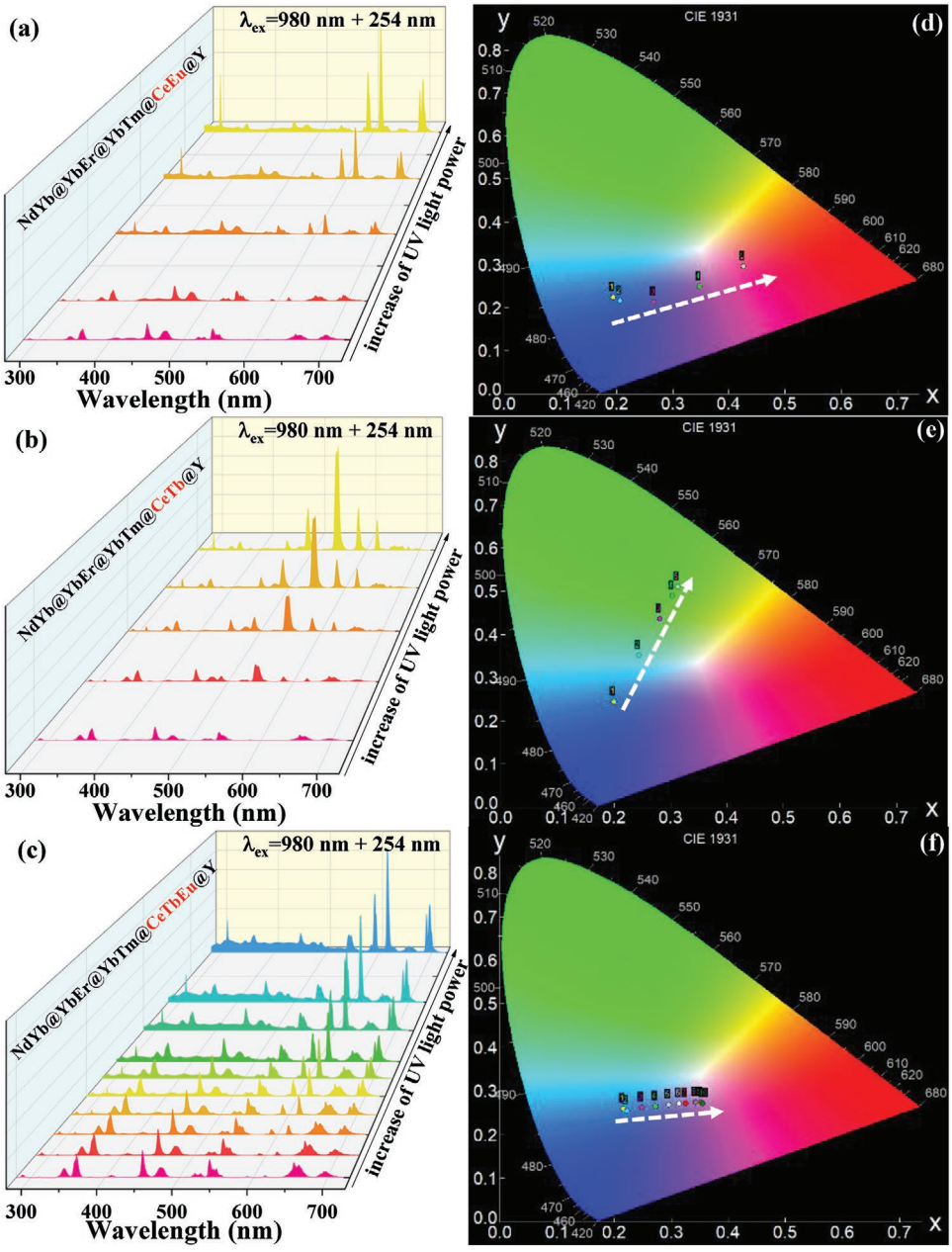

Figure 7. UC emission spectra for a) Ce/Eu, b) Ce/Tb, c) Ce/Tb/Eu-doped CSSSS samples under concurrent excitation of 980 nm laser and 254 nm UV lamp, where 980 nm laser power is fixed and UV lamp power is gradually elevated. d–f) UC emissive color coordinates in CIE diagrams of (a), (b), and (c).

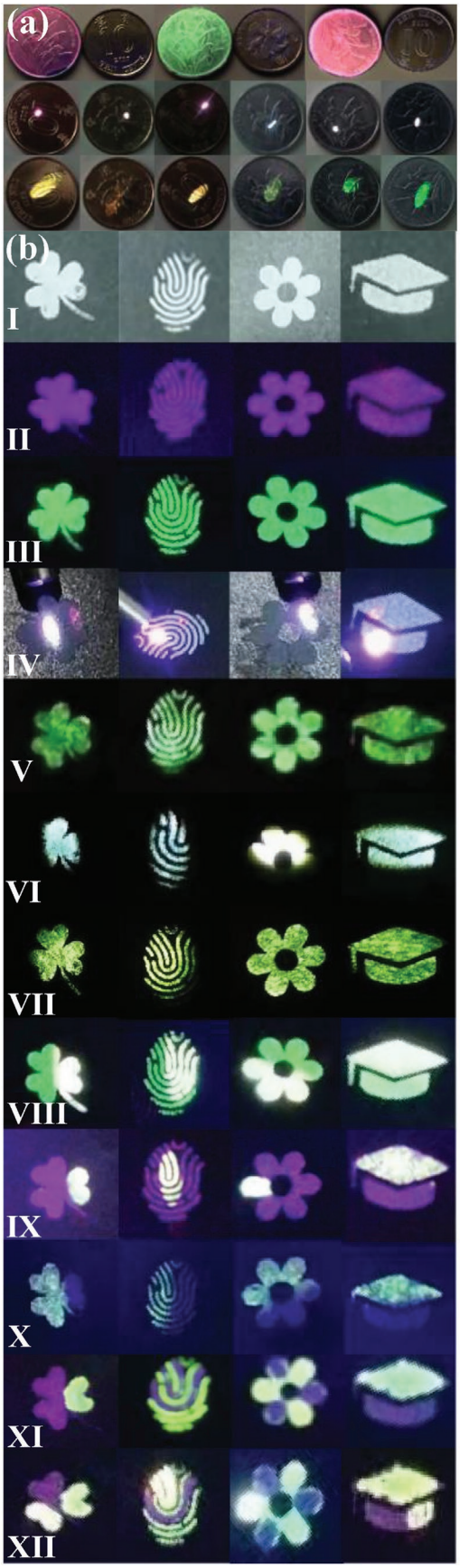

experiment, the CSSSS inks with UC/DS dual-modal luminescence were dropped on the surfaces of coins (**Figure 8**a). Upon UV light excitation, red, green and red DS emissive colors are discerned for the coins covered with Ce/Eu-, Ce/Tb-, and CeTb/Eu-doped CSSSS samples, respectively. As a comparison, without the addition of Ce sensitizers in third shell, DS luminescence is too weak to be detected. Meanwhile, distinct UC emissive colors are observable upon the irradiation of 980 nm focusing/defocusing laser. As tabulated in Table S11 in the Supporting Information, multiplex DS/UC luminescent colors for the CSSSS inks with multimodal excitations can be indeed used to distinguish different coins. In addition, we can design different patterns and print them on the paper or metal plate by using the as-prepared Ce/Eu doped and Ce/Tb doped CSSSS inks via the screen-printing technique. Similarly, characteristic DS/UC multicolor luminescence can be observed in all the patterns upon UV lamp or 980 nm laser (focusing or defocusing) excitation (Figure 8b). Particularly, we examine the possibility to realize dual-color luminescence in a sole pattern via simultaneous UV lamp and 980 nm laser excitation. As expected, green DS emissive color and white UC emissive color can be concurrently observed upon dual UV lamp and 980 nm focused laser excitation for the patterns constructed by Ce/Tb doped CSSSS inks; red DS emissive color and pink or green UC emissive color is detectable under the irradiation of UV lamp and 980 nm focusing or defocusing laser for the patterns constructed by Ce/Eu doped CSSSS inks; tricolor DS/UC emissions (green, pink, white) are visible by naked eyes for the patterns constructed by both Ce/Tb and Ce/Eu doped CSSSS inks. All these results verify these core@multishell nanoarchitectures with dual-modal excitable multicolor UC/DS combined luminescence are indeed suitable for high-level anticounterfeit and information encryption with facile decryption and authentication.

3. Conclusion

In summary, we have successfully prepared a series of $NaYF_4$: Nd/Yb@$NaYF_4$: Yb/Er@$NaGdF_4$: Yb/Tm@$NaGdF_4$: A@$NaYF_4$

Figure 8. a) DS luminescence for the CSSSS coated coins (from left to right: Ce/Eu, Eu, Ce/Tb, Tb, Ce/Tb/Eu, Tb/Eu doped CSSSS samples) under the irradiation of 254 nm UV lamp (first row). UC luminescence for the CSSSS coated coins (from left to right: Eu, Tb, Tb/Eu, Ce/Eu, Ce/Tb, Ce/Tb/Eu doped CSSSS samples) under the irradiation of 980 nm laser (second row: focusing laser, third row: defocusing). b) A series of luminescent patterns prepared by screen-printing technique using Ce/Tb-doped and Ce/Eu-doped CSSSS inks. I) Ce/Eu CSSSS patterns under daylight, II) Ce/Eu CSSSS patterns under irradiation of 254 nm UV lamp, III) Ce/Tb CSSSS patterns under irradiation of 254 nm UV lamp, IV) Ce/Eu CSSSS patterns under irradiation of 980 nm focusing laser, V) Ce/Eu CSSSS patterns under irradiation of 980 nm defocusing laser, VI) Ce/Tb CSSSS patterns under irradiation of 980 nm focusing laser, VII) Ce/Tb CSSSS patterns under irradiation of 980 nm defocusing laser, VIII) Ce/Tb CSSSS patterns under irradiation of 254 nm UV lamp and 980 nm focusing laser, IX) Ce/Eu CSSSS patterns under irradiation of 254 nm UV lamp and 980 nm focusing laser, X) Ce/Eu CSSSS patterns under irradiation of 254 nm UV lamp and 980 nm defocusing laser, XI) Ce/Tb and Ce/Eu CSSSS patterns under irradiation of 245 nm UV lamp, XII) Ce/Tb and Ce/Eu CSSSS patterns under irradiation of 245 nm UV lamp and 980 nm focusing laser.

(A = Eu, Tb, Tb/Eu, Ce/Eu, Ce/Tb, Ce/Tb/Eu) core@multishell NCs with simultaneous upconverting and downshifting dual-modal emissions. In these nanoarchitectures, Nd, Yb and Ce sensitizers enable to excite NCs via three diverse wavelengths (254, 980, or 808 nm); Er/Tm activators can produce RGB tricolor UC emissions via multiphoton energy transfer UC processes, and Eu/Tb activators can yield R/G UC or DS emissions via energy migration of Tm → Gd → Eu/Tb or Ce → Gd → Eu/Tb; the spatially confined separation of dopants in distinct shells avoids adverse interactions among different lanthanide ions and leads to intense UC/DS emissions. Importantly, the combined luminescence from Er/Tm/Eu/Tb UC emissions and Eu/Tb DS emissions is highly sensitive to the selected excitation modes, where a single UV (254 nm) light or NIR (980 or 808 nm) focusing/defocusing laser source can be employed or their combinations of xenon lamp and NIR laser are applicable. Benefited from multimodal excitable bi-functional emitting feature of Ln-doped core@multishell NCs, screen-printing multiple information encryption and anti-counterfeit with convenient decryption by appropriately choosing excitation modes are demonstrated. These findings verify great promise of the designed core@multishell nanoarchitectures for applications in high-level anticounterfeit and high-capacity information encryption and give new insights for development of advanced optoelectronic materials.

4. Experimental Section

Materials: All the raw materials, including yttrium chloride ($YCl_3{\cdot}6H_2O$, 99.9%), gadolinium chloride ($GdCl_3{\cdot}6H_2O$, 99.9%), neodymium chloride ($NdCl_3{\cdot}6H_2O$, 99.9%), ytterbium chloride ($YbCl_3{\cdot}6H_2O$, 99.9%), erbium chloride ($ErCl_3{\cdot}6H_2O$, 99.9%), thulium chloride ($TmCl_3{\cdot}6H_2O$, 99.9%), cerium chloride ($CeCl_3{\cdot}6H_2O$, 99.9%), europium chloride ($EuCl_3{\cdot}6H_2O$, 99.9%), terbium chloride ($TbCl_3{\cdot}6H_2O$, 99.9%), oleic acid (OA, 90%), 1-octadecene (ODE, 90%), ammonium fluoride (NH_4F, 99%), and sodium hydroxide (NaOH, 99%) were purchased from Sinopharm Chemical Reagent Company and were directly used without further refinement.

Synthesis of Core@Multishell NCs: Typically, to synthesize $NaYF_4$: Nd/Yb (30/30 mol%) core, 2 mmol of Y^{3+}, Yb^{3+} and Nd^{3+} in total were added to a 100 mL flask containing 12 mL OA and 30 mL ODE. The mixture was heated at 160 °C for 60 min before cooling down to 45 °C. Afterwards, 20 mL methanol solution containing NH_4F (6 mmol) and NaOH (5 mmol) was added and the resultant solution was stirred at 50 °C for 60 min. After the methanol was thoroughly evaporated, the solution was heated to 300 °C under N_2 protection for 1 h and then cooled down to room temperature. The core NCs were precipitated by addition of enough ethanol, collected by centrifugation at 10 000 rpm for 15 min, washed with ethanol for three times, and finally re-dispersed in 8 mL cyclohexane.

For the growth of different shells, similar procedure was performed. Merely one more step was inserted. That is, before the addition of NH_4F and NaOH, the pre-prepared core NCs dispersed in 8 mL cyclohexane was added to the above solution and kept at 110 °C for 30 min. The first shell was $NaYF_4$: Yb/Er with 60 mol% doping concentration for Yb^{3+} and 0.5 mol% for Er^{3+}; the second shell was $NaGdF_4$: Yb/Tm, where the concentrations of Yb^{3+} and Tm^{3+} are 57 and 3 mol%, respectively; The third shell $NaGdF_4$ have been doped with six sets of lanthanide ions, i.e., 1) 10 mol% Eu^{3+}, 2) 10 mol% Tb^{3+}, 3) 10 mol% Tb^{3+} and 10 mol% Eu^{3+}, 4) 20 mol% Ce^{3+} and 10 mol% Eu^{3+}, 5) 20 mol% Ce^{3+} and 10 mol% Tb^{3+}, and 6) 10 mol% Ce^{3+}, 10 mol% Tb^{3+}, and 10 mol% Eu^{3+}, respectively. The fourth shell was the inert $NaYF_4$ layer.

Characterizations: XRD patterns of NCs were recorded by a powder diffractometer (DMAX2500 RIGAKU) using Cu-K_a radiation (λ = 0.154 nm). Microstructures of all the prepared samples were studied using a scanning electron microscope (SEM, JSM-6700F). The sizes and morphologies of CSSSS samples were investigated via a transmission electron microscope (TEM, JEM-2010). The high-angle annual dark-field scanning transmission electron microscopy (HAADF-STEM) observations were carried out on a FEI aberration-corrected Titan Cubed S-Twin transmission electron microscope equipped with an energy dispersive X-ray spectroscope (EDS) operated at 200 kV. TEM and STEM specimens were prepared by directly dropping a dilute cyclohexane dispersion solution of CSSSS on a carbon coated copper grid. Unlike conventional TEM, the contrast in HAADF-STEM image was determined by the numbers of scattered electrons at high angles. In this technique, the high-angle scattering intensity has the characteristics of Rutherford scattering and is sensitive to atomic number (Z) contrast, scaling proportionally to $\approx Z^2$.[46–48] DS and UC emission spectra were recorded on an Edinburgh Instruments FLS1000 spectrofluorometer equipped with 980 and 808 nm lasers and a xenon lamp (450 W) as the excitation sources. UC quantum yield (ULQY) values for the investigated samples were determined by combining an integrated sphere in FLS1000 spectrofluorometer.Visible UC decay curves were measured in the same FLS1000 spectrofluorometer equipped with pulse 980 or 808 nm laser. NIR DS decay curves of Yb^{3+} were recorded with the Hamamatsu R5509 photomultiplier tube excited by a microsecond flash lamp (μF 900). All the measurements were carried out at room temperature.

Design of Anti-Counterfeiting Patterns and Characterizations: Security inks were made by mixing the as-prepared Ln-doped CSSSS NCs with commercial blank screen-printing ink (SND-100, purchased from ZHONGYI INK & PAINT CO., LTD, China). Using the above luminescent inks, a series of designed patterns were printed on black paper or metal plate. The DS/UC luminescence images were recorded by a camera (Canon, EOS 80D, EF-S 18–200 mm f/3.5-5.6 IS) in an all-manual mode and using a 980 nm focusing/defocusing laser and a 254 nm UV lamp as excitation sources. To identity different coins using CSSSS NCs, transparent NCs colloidal cyclohexane solutions were directly dropped on the surfaces of coins and dried at 60 °C for 10 min in the furnace.

Supporting Information

Supporting Information is available from the Wiley Online Library or from the author.

Acknowledgements

This work was supported by the National Natural Science Foundation of China (51972060).

Conflict of Interest

The authors declare no conflict of interest.

Keywords

anti-counterfeiting, core@shell, downshifting, lanthanide ions, luminescent materials, upconverting

Received: February 4, 2020
Revised: March 12, 2020
Published online: April 20, 2020

[1] Markets and Markets, Anti-Counterfeit Packaging Market Report, http://www.marketsandmarkets.com/PressReleases/anticounterfeit-market.asp (accessed: January 2017).
[2] T. Y. Sun, B. Z. Xu, B. Chen, X. Chen, M. Y. Li, P. Shi, F. Wang, *Nanoscale* **2017**, *9*, 2701.
[3] A. Sukhlecha, *Indian J. Pharmacol.* **2007**, *39*, 255.
[4] J. Andres, R. D. Hersch, J.-E. Moser, A. S. Chauvin, *Adv. Funct. Mater.* **2014**, *24*, 5029.
[5] X. Li, Y. Xie, B. Song, H.-L. Zhang, H. Chen, H. Cai, W. Liu, Y. Tang, *Angew. Chem., Int. Ed.* **2017**, *56*, 2689.
[6] M. Li, Y. Feng, Q. Tian, W. Yao, L. Liu, X. Li, H. Wang, W. Wu, *Dalton Trans.* **2018**, *47*, 11264.
[7] K. Takazawa, Y. Kitahama, Y. Kimura, G. Kido, *Nano Lett.* **2005**, *5*, 1293.
[8] R. Freeman, I. Willner, *Chem. Soc. Rev.* **2012**, *41*, 4067.
[9] N. M. Sangeetha, P. Moutet, D. Lagarde, G. Sallen, B. Urbaszek, X. Marie, G. Viau, L. Ressier, *Nanoscale* **2013**, *5*, 9587.
[10] J. Zhou, Y. Yang, C. Y. Zhang, *Chem. Rev.* **2015**, *115*, 11669.
[11] F. W. Kang, J. J. He, T. Y. Sun, Z. Y. Bao, F. Wang, D. Y. Lei, *Adv. Funct. Mater.* **2017**, *27*, 1701842.
[12] R. R. Deng, F. Qin, R. F. Chen, W. Huang, M. H. Hong, X. G. Liu, *Nat. Nanotechnol.* **2015**, *10*, 237.
[13] E. H. Song, X. X. Han, Y. Y. Zhou, Y. Wei, X. F. Jiang, S. Ye, B. Zhou, Z. G. Xia, Q. Y. Zhang, *iScience* **2019**, *19*, 597.
[14] W. J. Yao, Q. Y. Tian, W. Wu, *Adv. Opt. Mater.* **2019**, *7*, 1801171.
[15] X. Xu, B. B. Zhang, L. Jia, Y. P. Fan, R. J. Chen, T. H. Zhu, B. Z. Liu, *ACS Appl. Mater. Interfaces* **2019**, *11*, 35294.
[16] D. Zhou, D. Liu, W. Xu, X. Chen, Z. Yin, X. Bai, B. Dong, L. Xu, H. W. Song, *Chem. Mater.* **2017**, *29*, 6799.
[17] W. J. Yao, Q. Y. Tian, J. Liu, Q. W. Xue, M. X. Li, L. Liu, Q. Lu, W. Wu, *Nanoscale* **2017**, *9*, 15982.
[18] X. X. Han, E. H. Song, B. Zhou, Q. Y. Zhang, *J. Mater. Chem. C* **2019**, *7*, 8226.
[19] Y. T. Ren, Z. W. Yang, M. J. Li, J. F. Ruan, J. Y. Zhao, J. B. Qiu, Z. G. Song, D. C. Zhou, *Adv. Opt. Mater.* **2019**, *7*, 1900213.
[20] X. Y. Wu, E. K. L. Yeow, *Nanoscale* **2019**, *11*, 15259.
[21] C. L. Wang, Y. H. Jin, L. F. Yuan, H. Y. Wu, G. F. Ju, Z. Z. Li, D. Liu, Y. Lv, L. Chen, Y. H. Hu, *Chem. Eng. J.* **2019**, *374*, 992.
[22] B. Zhou, L. Yan, L. L. Tao, N. Song, M. Wu, T. Wang, Q. Y. Zhang, *Adv. Sci.* **2018**, *5*, 1700667.
[23] F. Auzel, *Chem. Rev.* **2004**, *104*, 139.
[24] F. Wang, X. G. Liu, *Chem. Soc. Rev.* **2009**, *38*, 976.
[25] X. Qin, X. W. Liu, W. Huang, M. Bettinelli, X. G. Liu, *Chem. Rev.* **2017**, *117*, 4488.
[26] C. Fink, K. E. Maskus, Y. Qian, *World Bank Res. Obs.* **2015**, *31*, 1.
[27] T. Blumenthal, J. Meruga, P. S. May, J. Kellar, W. Cross, K. Ankireddy, S. Vunnam, Q. N. Luu, *Nanotechnology* **2012**, *23*, 185305.
[28] D. Q. Chen, Y. L. Yu, H. Lin, P. Huang, F. Weng, Z. Shan, Y. S. Wang, *Opt. Lett.* **2009**, *34*, 2882.
[29] Z. G. Xia, R. S. Liu, *J. Phys. Chem. C* **2012**, *116*, 15604.
[30] Y. S. Liu, D. T. Tu, H. M. Zhu, R. F. Li, W. Q. Luo, X. Y. Chen, *Adv. Mater.* **2010**, *22*, 3266.
[31] Y. Wang, K. Zheng, S. Song, D. Fan, H. Zhang, X. Liu, *Chem. Soc. Rev.* **2018**, *47*, 6473.
[32] X. Chen, D. F. Peng, Q. Jiang, F. Wang, *Chem. Soc. Rev.* **2015**, *44*, 1318.
[33] D. M. Yang, P. A. Ma, Z. Y. Hou, Z. Y. Cheng, C. X. Li, J. Lin, *Chem. Soc. Rev.* **2015**, *44*, 1416.
[34] C. Homann, L. Krukewitt, F. Frenzel, B. Grauel, C. Wurth, U. Resch-Genger, M. Haase, *Angew. Chem., Int. Ed.* **2018**, *57*, 8765.
[35] H. Dong, L. D. Sun, C. H. Yan, *Chem. Soc. Rev.* **2015**, *44*, 1608.
[36] G. Y. Chen, H. Agren, T. Y. Ohulchanskyy, P. N. Prasad, *Chem. Soc. Rev.* **2015**, *44*, 1680.
[37] J. Liu, H. Rijckaert, M. Zeng, K. Haustraete, B. Laforce, L. Vincze, I. Van Driessche, A. M. Kaczmarek, R. Van Deun, *Adv. Funct. Mater.* **2018**, *28*, 1707365.
[38] Y. F. Wang, G. Y. Liu, L. D. Sun, J. W. Xiao, J. C. Zhou, C. H. Yan, *ACS Nano* **2013**, *7*, 7200.
[39] X. J. Xie, N. Y. Gao, R. R. Deng, Q. Sun, Q. H. Xu, X. G. Liu, *J. Am. Chem. Soc.* **2013**, *135*, 12608.
[40] F. Wang, J. Wang, X. G. Liu, *Angew. Chem., Int. Ed.* **2010**, *49*, 7456.
[41] F. Shi, S. Wang, X. S. Zhai, D. Zhao, W. P. Qin, *CrystEngComm* **2011**, *13*, 3782.
[42] Q. Cheng, J. Sui, W. Cai, *Nanoscale* **2012**, *4*, 779.
[43] W. Zheng, P. Huang, D. T. Tu, E. Ma, H. M. Zhu, X. Y. Chen, *Chem. Soc. Rev.* **2015**, *44*, 1379.
[44] G. Blasse, B. C. Grabmaier, *Luminescent Materials*, Springer Verlag, Berlin **1994**.
[45] Z. G. Xia, Q. L. Liu, *Prog. Mater. Sci.* **2016**, *84*, 59.
[46] S. I. Sanchez, M. W. Small, S. Sivaramakrishnan, J. G. Wen, J. M. Zuo, R. G. Nuzzo, *Anal. Chem.* **2010**, *82*, 2599.
[47] K. A. Abel, J. C. Boyer, C. M. Andrei, F. C. J. M. Van Veggel, *J. Phys. Chem. Lett.* **2011**, *2*, 185.
[48] D. Q. Chen, P. Huang, *Dalton Trans.* **2014**, *43*, 11299.